BL-8B/2013G001,BL-8B/2014G507, BL-9C/2013G068, BL-12C/2014G501,BL-12C/2014G506

Structural and electronic properties of Mn–Co hexacyanoferrates against Li

Yutaro Kurihara[1] and Yutaka Moritomo[1,2]
[1]Graduate School of Pure and Applied Science, University of Tsukuba, Tsukuba 305-8571, Japan
[2]Tsukuba Research Center for Interdisciplinary Materials Science (TIMS), University of Tsukuba, Tsukuba305-8571, Japan

1 Introduction

The PBAs, A_xM[Fe(CN)$_6$]$_z w$H$_2$O (A and M are alkali and transition metals, respectively.), are promising cathode materials for LIBs. Imanishi *et al.*[1,2] reported Li^+ intercalation behaviors in M[Fe(CN)$_6$]$_z$ (M = V, Mn, Fe, Ni, Cu). However, their charge/discharge cyclability is far from satisfactory. Cyclability is fairly improved in $K_{0.10}Mn^{II}[Fe^{III}(CN)_6]_{0.70}4.2H_2O$ and $Rb_{0.61}Mn^{II}[Fe^{III}(CN)_6]_{0.87}$-2.2H$_2$O.[3] Matsuda and Moritomo[4] synthesized a thin film of manganese hexacyanoferrate, $Li_{1.32}Mn^{II}[Fe^{II}(CN)_6]_{0.83}3.5H_2O$, by means of electrochemical deposition. They reported that the thin-film electrode exhibits a high capacity of 128mAh/g and an average operating voltage of 3.6V against Li with good cyclability. Kurihara *et al.*[5] improved the capacity of Mn-PBA by increasing the Fe concentration (z): the discharge capacity increases from 115mAh/g at z = 0.83 ($Li_{1.32}Mn^{II}[Fe^{II}(CN)_6]_{0.83}3.5H_2O$) to 143mAh/g at z = 0.93 ($Li_{1.72}Mn^{II}[Fe^{II}(CN)_6]_{0.93}2.3H_2O$). On the other hand, Takachi *et al.*[6] reported that the $Li_{1.60}Co^{II}[Fe^{II}(CN)_6]_{0.90}2.9H_2O$ film electrode exhibits a high capacity of 132mAh/g and an average operating voltage of 3.6V against Li with good cyclability.

The high capacity of Mn-PBA is ascribed to the two reduction processes for Mn and Fe,[7] which form two well defined plateaus at 3.8V (Mn) and 3.4V (Fe) in the discharge curve of LIB. On the other hand, the high capacity of Co-PBA is ascribed to two reduction processes for Fe and Co,[7] which form two plateaus at 4.0V (Fe) and 3.2V (Co) in the discharge curve of LIB. We note that the order of redox sites is reversed between the two systems; Mn➔Fe in Mn-PBA and Fe➔Co in Co-PBA. We also emphasize that the redox voltage (V_{Fe}) of Fe is markedly increased in Co-PBA (4.0 V) as compared with that (3.4 V) in Mn-PBA. In this study, we fabricated thin films of mixed PBAs, $Li_xMn_{1-y}Co_y$[Fe(CN)$_6$]$_z w$H$_2$O, and investigated their electrochemical, structural, and electronic properties against x.

2 Experiment

Thin films of $Na_xMn^{II}_{1-y}Co^{II}_y$[FeII(CN)$_6$]$_z wH_2$O were synthesized by electrochemical deposition on an indium–tin oxide (ITO) transparent electrode under potentiostatic conditions at 10.45V vs a standard Ag/AgCl electrode in an aqueous solution containing $K_3[Fe^{III}(CN)_6]$, $Mn^{II}Cl_2$, $Co^{II}Cl_2$, and 5 mol/L NaCl. The deposition time was 5 min. The thickness of the films was 0.5 μm. Before the film growth, the surface of the ITO electrode was purified by the electrolysis of water for 5 min. The chemical composition of the films was determined by inductively coupled plasma (ICP) measurement. The magnitudes of x and z were determined so as to minimize the sum of the squares of the residual error under the charge neutrality condition (x + 2 - 4z = 0). The Li compounds, $Li_xMn_{1-y}Co_y$[Fe(CN)$_6$]$_z w$H$_2$O, were obtained by the electrochemical substitution of Li^+ for Na^+. The substitutions was performed by charge/discharge cycles of the as-grown films in an ethylene carbonate (EC)/diethyl carbonate (DEC) solution containing 1 mol/L $LiClO_4$.

The Li concentration (x) of the film was controlled by the charge/discharge process described above. The magnitude of x was calculated from the total current under the assumption that Li_{4z-2}M[Fe(CN)$_6$]$_z$ is in the discharge state and $Li_{0.00}$M[Fe(CN)$_6$]$_z$ is in the charge state. Except for the high-x region, the film is stable in air. The high-x films were carefully and rapidly sealed in a glass capillary. The film was carefully removed from the ITO glass substrate with a microspatula, and then fine powder was filled into a 300μmϕ glass capillary. The powder diffraction pattern was detected with an imaging plate (IP). The exposure time was 5 min. The X-ray wavelength was calibrated using the lattice constant (a = 5.41112Å) of standard CeO_2 powder. Thus-obtained power diffraction patterns were analyzed by the Rietveld method (Rietan-FP[8]).

Ex situ XAS measurements were performed at the 9C beamline of the PF, KEK. XAS spectra were measured in a fluorescent yield mode with a Lytle detector at 300 K. The X-ray was monochromized with a Si(111) double-crystal monochromator. In the XAS measurement for respective elements, e.g., Mn, Co, and Fe, the monochromator was calibrated by the K-edge of the respective metal foils. The background subtraction, normalization, and component decomposition were performed with the ATHENA program.[9] The self-absorption effect is negligible because the penetration depths (λ> 40μm) of the compounds at the fluorescence and absorption energies of the Mn, Fe, and Co K-edges are much larger than the thickness of the films (= 0.5 μm)

3 Results and Discussion

Figure 1(a) shows the XRD patterns of $Li_xMn_{0.89}Co_{0.11}$[Fe(CN)$_6$]$_{0.89}$3.1H$_2$O (y = 0.11) against x. Except at x =0.00, the XRD patterns can be indexed with the fcc setting. The cell parameter a was refined by Rietveld analysis with the fcc (Fm3̲m: Z = 4) model. At x = 0.00, doublet features are observed in the (200), (220), and (400) reflections. The features indicate a phase

separation into two fcc phases. The cell parameter a of the respective phase was refined with a two-phase model. Similar two-phase features are observed in the low-x region at y = 0.22 (not shown).

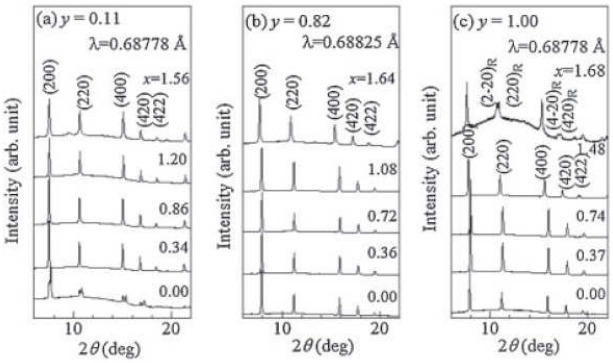

Fig. 1 XRD patterns of (a) $Li_xMn_{0.89}Co_{0.11}[Fe(CN)_6]_{0.89}3.1H_2O$, (b) $Li_xMn_{0.18}Co_{0.82}[Fe(CN)_6]_{0.91}3.4H_2O$, and (c) $Li_xCo[Fe(CN)_6]_{0.92}4.6H_2O$. Values in parentheses represent indexes in the fcc setting. The subscript R indicates the rhombohedral setting

Figure 1(b) shows the XRD patterns of $Li_xMn_{0.18}Co_{0.82}[Fe(CN)_6]_{0.91}3.4H_2O$ (y = 0.82). All the XRD patterns can be indexed with the fcc setting. The cell parameter a was refined with the fcc (Fm3m: Z = 4) model. Figure 1(c) shows the XRD patterns of $Li_xCo[Fe(CN)_6]_{0.92}4.6H_2O$ (y = 1.00). Except at x = 1.68, the XRD patterns can be indexed with the fcc setting. The cell parameter a was refined with the fcc (Fm3m: Z = 4) model. At x = 1.68, a doublet feature is observed at 11°, indicating a rhombohedral distortion. The cell parameters a and c at x = 1.68 were refined with the rhombohedral (R$\bar{3}$m: Z = 4) model.

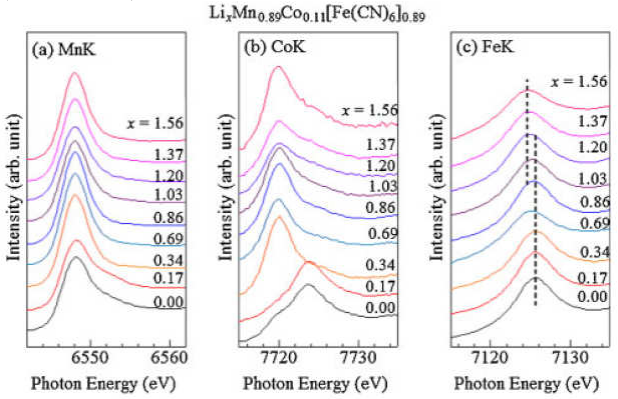

Fig. 2. XAS of $Li_xMn_{0.89}Co_{0.11}[Fe(CN)_6]_{0.89}3.1H_2O$ against x around the (a) Mn K-, (b) Co K-, and (c) Fe K-edges. The broken vertical lines in (c) represent the peak energies of Fe^{2+} and Fe^{3+}.

Figure 2(a) shows the XAS spectra of $Li_xMn_{0.89}Co_{0.11}[Fe(CN)_6]_{0.89}3.1H_2O$ (y = 0.11) against x around the Mn Kedge. The spectra show negligible changes with x, indicating that the Mn valence essentially remains 2+. Figure 2(b) shows the XAS spectra of the films against x around the Co K-edge. The XAS spectrum at **x** = 0.0 nearly coincides with that of low-spin (LS) Co^{3+}, while the spectrum at 1.56 coincides with that of HS Co^{2+}.The systematic spectral change in Fig. 2(b) indicates that the average Co valence changes from 3+ to 2+ with an increase in x. Figure 6(c) shows the XAS spectra of the films against x around the Fe K-edge. The broken vertical lines represent the peak energies of Fe^{2+} and $Fe3^{+}$. The red shift of the peak indicates that the average Fe valence changes from 3+ to 2+ with an increase in x.

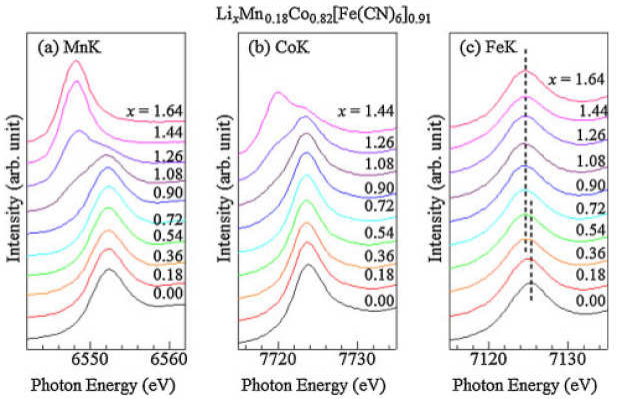

Fig. 3. X-ray absorption spectra of $Li_xMn_{0.18}Co_{0.82}[Fe(CN)_6]_{0.91}3.4H_2O$ against x around the (a) Mn K-, (b) Co K-, and (c) Fe K-edges. The broken vertical lines in (c) represent the peak energies of Fe^{2+} and Fe^{3+}.

Figure 3(a) shows the XAS spectra of $Li_xMn_{0.18}Co_{0.82}[Fe(CN)_6]_{0.91}3.4H_2O$ (y = 0.82) against x around the Mn K-edge. The XAS spectrum at x = 0.0 is due to Mn^{3+}, while the spectrum at 1.64 is due to Mn^{2+}. The spectral change in Fig. 3(a) indicates that the average Mn valence changes from 3+ to 2+ with an increase in x. Figure 3(b) shows the XAS spectra of the films against x around the Co K-edge. The spectral change indicates that the average Co valence changes from 3+ to 2+ with an increase in x. Figure 3(c) shows the XAS spectra of the films against x around the Fe K-edge. The red shift of the peak indicates that the average Fe valence changes from 3+ to 2+ with an increase in x.

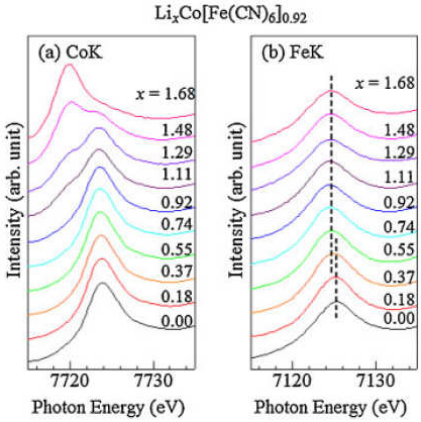

Fig. 4. X-ray absorption spectra of $Li_xCo[Fe(CN)_6]_{0.92}4.6H_2O$ against x around the (a) Co K- and (b) Fe Kedges. The broken vertical lines in (b) represent the peak energies of Fe^{2+} and Fe^{3+}.

Figure 4(a) shows the XAS spectra of $Li_xCo[Fe(CN)_6]_{0.92}4.6H_2O$ (y = 1.00) against x around the Co K-edge. The spectral change indicates that the average Co valence changes from 3+ to 2+ with increase in x. Figure 4(b) shows the XAS spectra of the films against x around the Fe K-edge. The red shift of the peak indicates that the average Fe valence changes from 3+ to 2+ with an increase in x.

Acknowledgement (option)
We thank M. Takachi for fruitful discussion on the lattice effects on the redox process. This work was supported by the Mitsubishi Foundation, the Canon Foundation, and a Grant-in-Aid for Scientific Research (Nos. 25620036 and 23249) from the Ministry of Education, Culture, Sports, Science and Technology, Japan. The elementary analysis of the films was performed at the Chemical Analysis Division, Research Facility Center for Science and Engineering, University of Tsukuba.

References

[1] N. Imanishi, *et al*., *J. Power Sources* **79**, 215 (1999).
[2] N. Imanishi, *et al*., *J. Power Sources* **81–82**, 530 (1999).
[3] M. Okubo, *et al*., *J. Phys. Chem. Lett.* **1**, 2063 (2010).
[4] T. Matsuda and Y. Moritomo, *Appl. Phys. Express* **4**, 047101 (2011).
[5] Y. Kurihara, T. Matsuda, and Y. Moritomo, *Jpn. J. Appl. Phys.* **52**, 017301 (2013).
[6] M. Takachi, T. Matsuda, and Y. Moritomo, *Jpn. J. Appl. Phys*. **52**, 044301 (2013)
[7] Y. Moritomo, M. Takachi, Y. Kurihara, and A. Matsuda, *Adv. Mater. Sci. Eng.* **2013**, 967285 (2013).
[8] F. Izumi and K. Momma, *Solid State Phenom.* **130**, 15 (2007).
[9] B. Ravel and M. Newville, *J. Synchrotron Radiat*. **12**, 537 (2005).

* moritomo.yutaka.gf@u.tsukuba.ac.jp